Combustion and Flame 256 (2023) 112995

Contents lists available at ScienceDirect

Combustion and Flame

journal homepage: www.elsevier.com/locate/combustflame

Impact of the injector lateral offset on the dynamics of a lean premixed flame and the thermoacoustic stability of a burner

S. Herff[a,*], K. Pausch[a], A. Lintermann[a], W. Schröder[b,c]

[a] Jülich Supercomputing Centre, Forschungszentrum Jülich GmbH, Wilhelm-Johnen-Str., Jülich 52425, Germany
[b] Institute of Aerodynamics RWTH Aachen University, Wüllnerstraße 5a, Aachen 52062, Germany
[c] JARA Center for Simulation and Data Science, RWTH Aachen University, Seffenter Weg 23, Aachen 52074, Germany

ARTICLE INFO

Article history:
Received 13 January 2023
Revised 26 July 2023
Accepted 27 July 2023

Keywords:
Thermoacoustic instability
Injector position
Asymmetric flame
Large-eddy simulation
Premixed flame

ABSTRACT

The response of a laminar lean premixed flame to excitations based on its position in the combustion chamber and the stability of a burner are numerically investigated. A finite-volume large-eddy simulation method is used to solve the compressible Navier-Stokes equations and a combined G-equation progress variable approach is used to model the flame. Various injector positions in the combustion chamber are investigated in a computational setup with an acoustically non-reflecting outflow boundary condition to analyze the impact on the response of the flame to an external excitation. Due to the changes in the flow field the shape of the flames depends on the displacement offset of the injector. Consequently, the instantaneous, local distribution of the heat release rate fluctuations which is caused by wrinkles on the flame surface is determined by the position of the injector. The heat release rate fluctuations are the dominant source of sound in the investigated configurations. Due to the discrepancies in the local heat release rate fluctuations the flame response to an excitation depends on the lateral offset of the injector. The overall trend of the integrated heat release is the same in most configurations, however, the phase is significantly altered. Since the phase angle of the response of the flame to an excitation determines the stability of a burner, self-excited instabilities can be avoided by adjusting the position of the injector. This is demonstrated using a modified computational domain with an acoustically reflecting outflow boundary condition, which causes the burner to have an acoustic quarter-wave eigenmode. Based on the results of the previous analysis of the flame responses, two injector positions in the combustion chamber are chosen such that the response of the flames is mutually phase-shifted by approximately π. Therefore, it is expected that one of the configurations will lead to a stable burner while the other one exhibits a self-excited instability. The results show that the injector position determines the stability of the burner configuration for the investigated flames.

1. Introduction

To reduce pollutant emissions, modern combustion facilities are operated at lean premixed combustion. However, the lean premixed combustion regime is prone to combustion instabilities which can cause an inefficient operation or in the worst case lead to the structural failure of the burner assembly [1]. Combustion instabilities can origin from a resonant coupling of the acoustic emission of the flame with the acoustic modes of the combustion chamber. That is, when the pressure oscillations in the combustion chamber and the acoustic emission of the flame are in phase self-excited instabilities occur in the burner configuration.

To determine the stability of a burner during the design stage the response of the flame to excitations is of major interest. The linear flame response to acoustic disturbances is often expressed as the flame transfer function (FTF) which describes the heat release fluctuations of the flame being caused by velocity fluctuations of the upstream flow. Low-order models to predict or control combustion instabilities are often based on FTFs. They can be determined experimentally [2,3], numerically [4], or by modeling approaches [5–7]. The details of the investigated configuration can have a significant impact on the FTF which was shown, e.g., in the study of Duchaine et al. [8] which focused on the susceptibility of the FTF to various parameters. However, the FTF is usually determined for single flames which are located either in an open environment or in a symmetric position in a combustion chamber. In Cuquel et al. [2] the effect of the confinement ratio of the com-

* Corresponding author.
E-mail address: s.herff@fz-juelich.de (S. Herff).

https://doi.org/10.1016/j.combustflame.2023.112995

bustion chamber on the FTF of a symmetric confined flame was shown. The results showed that a transposition of the FTF of an open or confined flame is required when the ratio of confinement of the symmetric confined flame changes.

In recent studies, a significant impact of non-symmetries in the configuration on the flame dynamics was shown. In Æsøy et al. [9], the effect of non-symmetry was investigated using a multi-flame combustor by changing the convection speed of adjacent flames. They found that the non-symmetry could be used to modify the response of the interacting flames. In Herff et al. [10] an unconfined, a symmetric confined, and a non-symmetric confined swirl flame were investigated to analyze the impact of confinement on the flow field and the dynamics of the flame. It was shown that the limit-cycle amplitude of a self-excited instability in the confined configurations was significantly reduced in the non-symmetric configuration. This result indicates that the position of the injector in the combustion chamber can determine the stability of a burner configuration. However, due to the complexity of the burner configuration a definite conclusion of the responsible mechanism could not be provided.

To analyze the effect of non-symmetric confinement on the flame response to acoustic excitations in detail, the current study focuses on a simpler configuration, i.e., a single laminar jet flame, which can be investigated much more efficiently. Since the flame response to acoustic disturbances, e.g., in the form of FTFs, is used to predict combustion instabilities, the results of the analysis of the generic configuration of this study are of significant relevance for engineering applications. In Pausch et al. [11] a similar configuration was used to investigate the acoustic source mechanisms of a symmetric confined flame. To be able to vary the position of the injector in the combustion chamber, the width of the combustion chamber of the configuration is increased in this study. Due to the confinement variation, the acoustic wave converts to a vorticity mode which can cause wrinkles of the flame surface. One symmetric configuration and three non-symmetric configurations are investigated. The comparison of the results of the four configurations shows the impact of the position of the injector on the response of the flame to acoustic excitations. Based on the findings two injector positions are considered in a modified setup to demonstrate that the stability of a burner depends on the position of the flame in the combustion chamber.

The numerical approach is based on the G-equation, which has been extensively used to model and analyze flame dynamics in various investigations. A comprehensive overview of these studies is beyond the scope of this discussion, however, a few studies which are relevant for the present investigation are given in the following. In Schuller et al. [5], it was shown that the flame motion and, noteworthy, the phase of the flame response can be captured by combining an accurate computation of the velocity field with a non-linear treatment of the flame motion based on the G-equation. The effect of stretch on the wrinkle amplitudes of acoustically excited premixed flames was analyzed in Wang et al. [12]. It was found that the wrinkle amplitudes can decay from the flame base to the tip due to stretch effects for a certain range of excitation frequencies. In Kashinath et al. [13], the impact of the perturbation velocity field on the nonlinear limit-cycle instabilities of a symmetrical premixed flame was analyzed. They showed that the convective speed of velocity perturbations is not generally the mean flow velocity which can significantly impact thermoacoustic instabilities. In Albayrak and Polifke [14], a G-equation approach was used to analyze the effect of non-uniform equivalence ratio on the flame response. They concluded that the phase of the flame response can be modified by non-uniform equivalence ratio perturbations. In the analytical study by Li et al. [15] the effect of asymmetry on the response of a two-dimensional flame to disturbances was analyzed. They found that the flame acts as a bandpass filter for transversal acoustic excitations due to cancellation effects of the two flame flanks. In contrast to the current study, the asymmetry in [15] was achieved by a non-zero transversal mean flow velocity and transversal flow perturbations were used to excite the flames. Note that these discrepancies in the flame configurations of the study by Li et al. with the current study leads to differences in the overall flame response and the mechanisms affecting the flame response. Furthermore, the G-equation approach has been used, e.g., in Matalon and Matkowsky [16], for the modeling of turbulent combustion.

The study is structured as follows. First, the numerical methods are introduced before the burner geometry and the numerical configurations are discussed. Then, the results of the four investigated configurations are analyzed and the effect of the injector position on the stability of a burner is shown for two configurations in a modified numerical setup. Finally, conclusions are drawn.

2. Numerical methods

A conservative finite-volume method for the solution of the Navier-Stokes equations coupled with a level-set solver for the G-equation is presented. Both methods have been introduced in [17] and are features of the in-house developed multi-physics simulation framework m-AIA (multiphysics Aerodynamisches Institut Aachen) [18].

The two-dimensional unsteady compressible Navier-Stokes equations are solved using the combined G-equation progress variable modeling approach by Moureau et al. [19] to compute the laminar lean premixed flame.

The governing equations read

$$\frac{\partial \boldsymbol{Q}}{\partial t} + \nabla \cdot \boldsymbol{H} = \dot{\boldsymbol{W}}, \tag{1}$$

where $\nabla = [\frac{\partial}{\partial x}, \frac{\partial}{\partial y}]^T$ is the vector of spatial derivatives in the Cartesian coordinate system with directions x and y. The vector of conservative variables $\boldsymbol{Q}$ and the flux vector $\boldsymbol{H}$, which is decomposed into an inviscid $\boldsymbol{H}^i$ and a viscous part $\boldsymbol{H}^v$, read in non-dimensional form

$$\boldsymbol{Q} = \begin{pmatrix} \rho \\ \rho \boldsymbol{v} \\ \rho E \\ \rho c \end{pmatrix}, \qquad \boldsymbol{H} = \boldsymbol{H}^i - \boldsymbol{H}^v = \begin{pmatrix} \rho \boldsymbol{v} \\ \rho \boldsymbol{v}\boldsymbol{v} + p\underline{\boldsymbol{I}} \\ \boldsymbol{v}(\rho E + p) \\ \rho \boldsymbol{v} c \end{pmatrix} + \frac{1}{Re_0} \begin{pmatrix} 0 \\ \underline{\boldsymbol{\tau}} \\ \underline{\boldsymbol{\tau}}\boldsymbol{v} + \boldsymbol{q} \\ \boldsymbol{J}_c \end{pmatrix}. \tag{2}$$

The quantity $\underline{\boldsymbol{I}}$ is the unit matrix, ρ denotes the density, $\boldsymbol{v} = [u_x, u_y]^T$ the velocity vector, E the total specific energy, c the progress variable, p the pressure, $\underline{\boldsymbol{\tau}}$ the stress tensor, $\boldsymbol{q}$ the vector of heat conduction, and $\boldsymbol{J}_c$ the diffusive flux of the progress variable. The Reynolds number $Re_0 = (\rho_0 a_0 l)/\mu_0$ is based on the characteristic length l and the speed of sound a_0, the density ρ_0, and the dynamic viscosity μ_0 at rest which is denoted by the subscript 0. The non-dimensionalization of the variables is done by $\rho_0 a_0^2$ for the pressure, a_0 for the velocity, ρ_0 for the density, and $t_0 = l/a_0$ for the time.

The evolution of the G-field is defined by the G-equation [20,21]

$$\frac{\partial G}{\partial t} + \left(\boldsymbol{v} + \frac{\rho_\infty^u}{\rho} s_{t,u} \boldsymbol{n} \right) \cdot \nabla G = 0, \tag{3}$$

where the normal vector

$$\boldsymbol{n} = -\frac{1}{|\nabla G|} \left(\partial G/\partial x,\ \partial G/\partial y \right)^T \tag{4}$$

points towards the unburnt fuel-air mixture. The zero-value level-set contour $G = G_0 = 0$ describes the motion of the inner-layer

temperature contour of the flame and the scalar G is defined to be positive in the burnt gas and negative in the unburnt gas. The flame speed is modeled by the laminar flame speed $s_{l,0}$ corrected by the product of the curvature $\kappa = \nabla \cdot \boldsymbol{n}$ and the Markstein length l_c

$$s_{t,u} = s_{l,0}\left(1 - \kappa l_c\right). \tag{5}$$

Note that hydrodynamic strain effects on the flame speed are neglected by the combustion model which limits the model to moderate flame stretch without local flame extinction on the flame surface. The combustion model is valid in the thin reaction zone and the corrugated flamelet regime [21]. Further details on the G-equation, the combustion model, and the modeling of the flame speed are discussed in Pitsch [21].

For further details, the reader is referred to the description of the numerical methods and the references in [10].

3. Numerical burner configurations

In the following, the computational setups are explained. In Sections 4.1 and 4.2 four configurations are considered which share common properties of the computational domain. That is, the formulation of the boundary conditions, the geometric parameters of the injector, and the geometric parameters of the combustion chamber are alike. The four configurations are characterized by the position of the flame, i.e., the position of the injector with respect to the centerline of the combustion chamber. A detailed description of all configurations is given below.

A not-to-scale schematic of the computational domain, which shows the common properties of the four configurations including the boundary conditions, is shown in Fig. 1.

The lean mixture of methane and air with an equivalence ratio of $\phi = 0.9$ enters the domain through an injector with the width $D = 8\,\text{mm}$ and the length $4D$. The Reynolds number based on the injector width and the average inflow velocity is $Re_\text{D} = 569$. The boundaries of the injector are formulated as adiabatic no-slip walls until they reach the boundaries of the combustion chamber. The combustion chamber has a width of $3D$ and a length of $14D$ leading to a total domain length of $L_\text{Domain} = 18D$. The boundaries of the combustion chamber are formulated as adiabatic slip walls to exclude effects that could be caused by the boundary layer at the combustion chamber walls. The outflow boundary condition is formulated as a non-reflecting Navier-Stokes characteristic boundary condition (NSCBC) [22], which reduces the acoustic reflections at the boundary. A linear relaxation coefficient as suggested by Rudy and Strikwerda [23] is used to avoid a drift of the imposed mean pressure. The microphone position 'MP' is used to record the pressure data. It is located $4D$ downstream of the injector exit. Note that a similar configuration was recently used in [11] to investigate the sound mechanisms of lean premixed flames. In contrast to the configurations in [11], the width of the combustion chamber is increased to enable the variation of the position of the injector. Noteworthy, the acoustic modes in the current investigation transition to a vorticity mode due to the resulting confinement jump which can cause wrinkles on the flame surface. Due to the Cartesian formulation, the investigated configurations correspond to slot flames. For conical flames, the qualitative results are expected to be similar while the quantitative findings will differ.

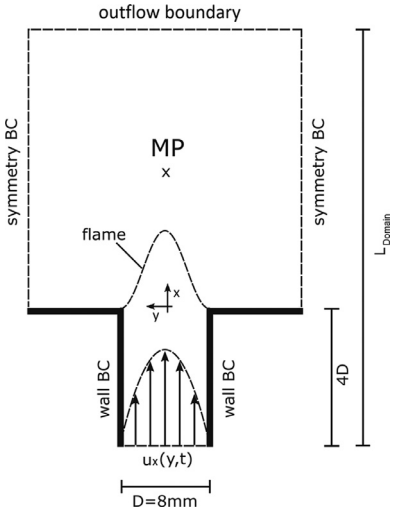

Fig. 1. Not-to-scale schematic of the geometry of the computational domain. The origin of the coordinate system is located on the centerline at the exit of the injector. The point denoted as 'MP' shows the microphone position, at which the pressure data is recorded.

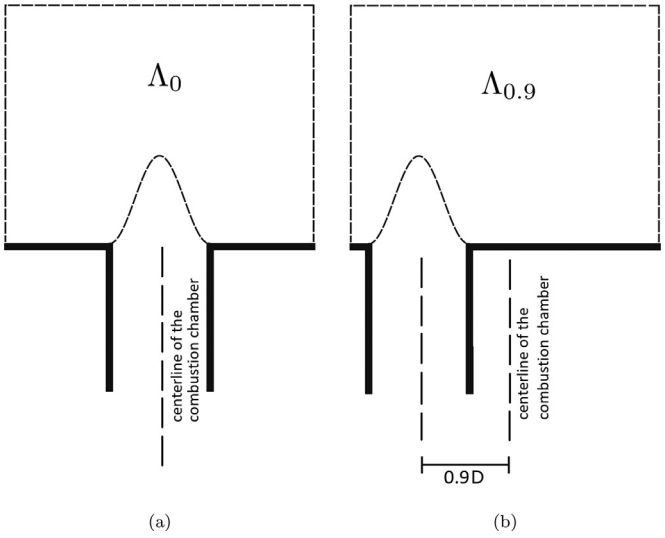

Fig. 2. Not-to-scale schematics of the injector positions in the combustion chambers of the Λ_0 (a) and the $\Lambda_{0.9}$ (b) configurations.

To investigate the impact of the flame position in the combustion chamber, four injector positions are considered. The notation of a configuration Λ_d indicates that the position of the injector has an offset of $d \cdot D$ from the centerline of the combustion chamber, where $d \in \{0, 0.3, 0.6, 0.9\}$. That is, the flame in configuration Λ_0 is located in the center of the combustion chamber and the flame in configuration $\Lambda_{0.9}$ is located close to the combustion chamber wall. Not-to-scale schematics of the injector positions of the Λ_0 and the $\Lambda_{0.9}$ configurations are shown in Fig. 2.

First, the steady-state solutions of the four configurations are computed. Then, the flames are excited by varying the inflow velocity using a sine function $u_x(y,t) = u_x(y) \cdot (1 + a \cdot \sin(2\pi f t))$, where $u_x(y)$ is a parabolic velocity profile, f is the excitation frequency, and a is the excitation amplitude. To investigate the response of the flames to external excitation the frequencies $f \in \{50\text{Hz}, 100\text{Hz}, 200\text{Hz}, 300\text{Hz}, 400\text{Hz}\}$ and the excitation amplitudes $a \in \{0.1, 0.25\}$ are considered. Note that these excitation amplitudes cause flame responses in the non-linear regime, which is typical for self-excited limit-cycle instabilities. Two excitation amplitudes are chosen to show that the results are valid for a wide range in the non-linear regime. To validate that the results of this study can be used to predict the linear stability behavior of a burner, this study should be extended to the linear regime by additional simulations. To investigate the effect in the linear regime, the excitation amplitude has to be significantly reduced especially for higher excitation frequencies. An overview of the configurations of the excited flames is given in Table 1.

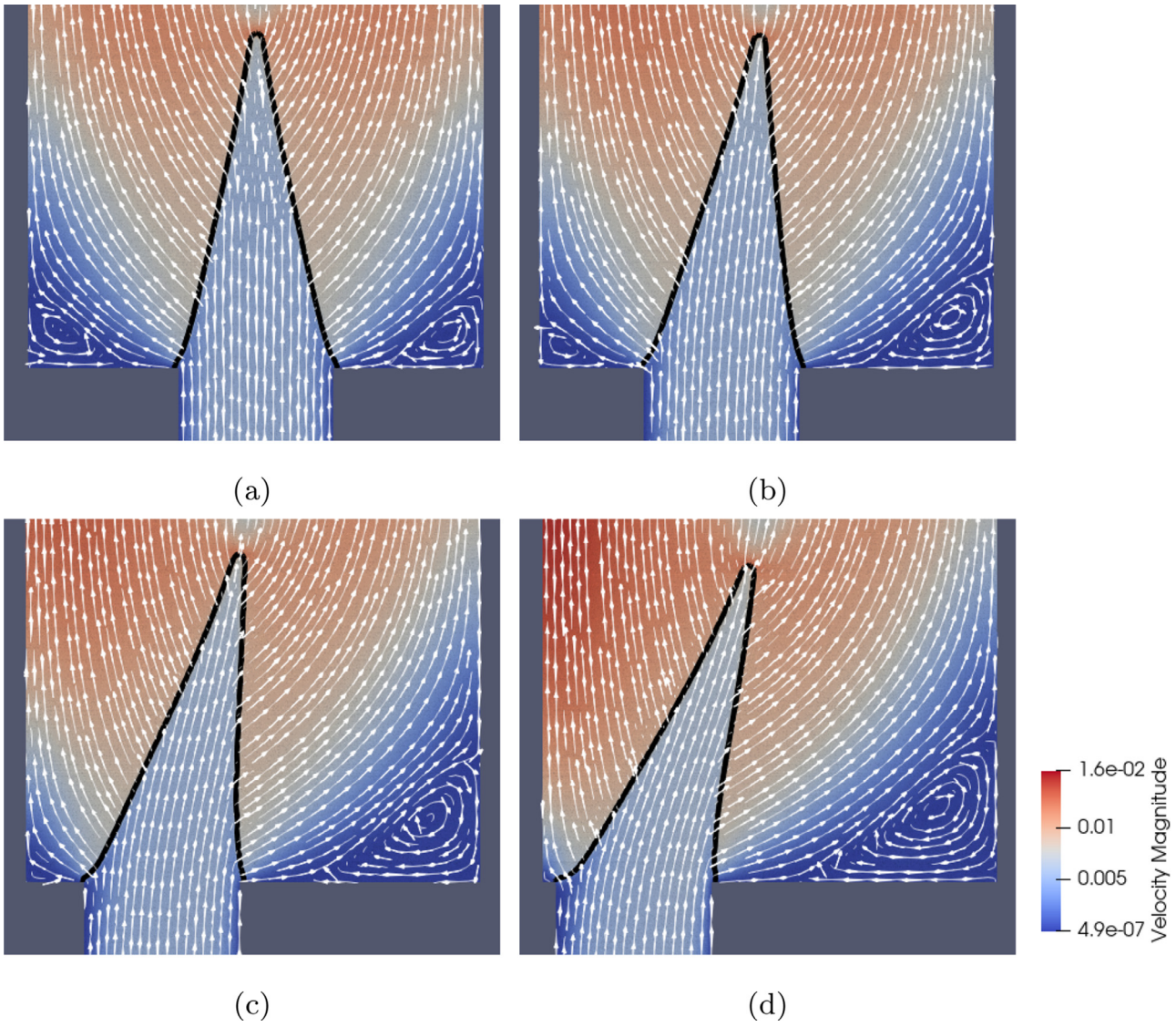

Fig. 3. Contours of the velocity magnitude of the steady-state solutions of the non-excited flames; Λ_0 configuration (a), $\Lambda_{0.3}$ configuration (b), $\Lambda_{0.6}$ configuration (c), and $\Lambda_{0.9}$ configuration (d). Streamlines are shown by the white arrows and the flame front is illustrated by the black contour which corresponds to $c = 0.5$.

Table 1
Overview of the configurations of the excited flames; equivalence ratio ϕ, Reynolds number based on the injector diameter and the bulk velocity Re_D, excitation amplitudes a relative to the inflow bulk velocity, excitation frequencies f, and ratio of flame length to convective wave length based on the inflow bulk velocity $\frac{l_f}{\lambda_{bulk}}$.

Notation	Setup Description	ϕ	Re_D	a	f[Hz]	$\frac{l_f}{\lambda_{bulk}}$
Λ_0	centered position of the flame	0.9	569	0.1, 0.25	50, 100, 200, 300, 400	0.75, 1.5, 3.0, 4.5, 6.0
$\Lambda_{0.3}$	the flame has a 0.3D offset from the centerline	0.9	569	0.1, 0.25	50, 100, 200, 300, 400	0.75, 1.5, 3.0, 4.5, 6.0
$\Lambda_{0.6}$	the flame has a 0.6D offset from the centerline	0.9	569	0.1, 0.25	50, 100, 200, 300, 400	0.75, 1.5, 3.0, 4.5, 6.0
$\Lambda_{0.9}$	the flame has a 0.9D offset from the centerline	0.9	569	0.1, 0.25	50, 100, 200, 300, 400	0.75, 1.5, 3.0, 4.5, 6.0

In Sections 4.1 and 4.2, the setup is used to analyze the impact of the flame position on its response to acoustic excitations. To subsequently investigate the effect on the thermoacoustic stability a modified numerical setup is used in Section 4.3. The modified configuration uses the computational domain shown in Fig. 1. However, the outflow boundary is not formulated as an NSCBC. Instead, a Dirichlet boundary condition for the pressure is used. That is, the outflow boundary is acoustically reflecting and corresponds to the boundary condition of a more realistic burner configuration. Furthermore, the length of the computational domain is massively increased to $L_{\text{Domain}} = 77D$ such that this configuration is a burner with a quarter-wave frequency of 400Hz.

4. Results

The impact of the position of the injector in the combustion chamber on the response of the flame to an external excitation is investigated. In Section 4.1, the flame shapes of steady flames and acoustically excited flames are discussed for four injector positions before their response to excitations with various excitation frequencies and excitation amplitudes is analyzed in Section 4.2. Then, the effect of the findings from Section 4.2 on the stability of a burner is shown for a burner configuration with more engineering boundary conditions by analyzing the stability of the burner for specific injector positions in Section 4.3.

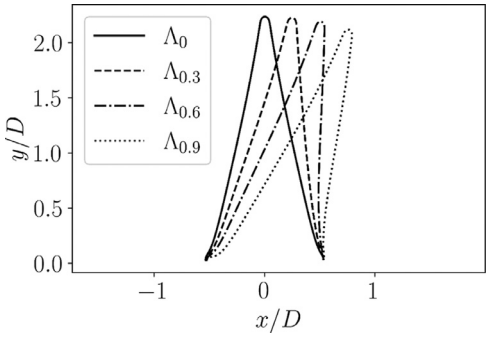

Fig. 4. Flame shapes of the steady-state solutions.

4.1. Flame shapes and wrinkles

The velocity fields, streamlines, and flame contours of the steady-state solutions are shown in Fig. 3. Note that all figures of the velocity magnitude contours use the same scaling. Recirculation zones are evident near the combustion chamber walls of the symmetric configuration Λ_0 (a). Due to the reduced distance between the injector and the combustion chamber wall the left recirculation zone is smaller in the $\Lambda_{0.3}$ configuration and does not exist in the higher lateral offset configurations $\Lambda_{0.6}$ and $\Lambda_{0.9}$. Simultaneously, the size of the right recirculation zone increases with the lateral injector offset. A juxtaposition of the flame shapes of the four configurations is shown in Fig. 4. The flame in the symmetric configuration Λ_0 has a length of approximately $l_f = 2D$. The resulting ratio of the flame length l_f to the convective wave length λ_{bulk} is listed for all configurations in Table 1. Evidently, in the configurations with an offset of the injector position with respect to the combustion chamber $\Lambda_{0.3}$, $\Lambda_{0.6}$, and $\Lambda_{0.9}$ the flame is inclined due to the streamline curvature in the mean flow caused by the previously discussed recirculation zones. The angle between the centerline of the injector and the line from the center of the injector to the tip of the flame increases with the offset of the injector position. Consequently, the lengths of the flanks of the flames differ for each configuration.

The contours of the instantaneous velocity magnitude and the flame front of the excited flames are shown in Figs. 5 and 6 at various excitation frequencies. The results for the excitation amplitude $a = 0.25$ are shown since the impact on the wrinkles is more obvious due to the slightly higher amplitude of the wrinkles. The qualitative results are the same for the excitation amplitude $a = 0.1$. The results for the lower excitation frequencies $f = 50$ Hz and $f = 100$ Hz are shown in Fig. 5. The high wavelength of the excitation causes a movement of the entire flame. Consequently, no wrinkles are observed in the surfaces of these flames. Note that the flame shape is already deformed for the frequency $f = 100$ Hz. Except for the deflection of the flame, which was discussed for the steady flames, the impact of the injector position on the dynamics of the flames is low in these configurations. This will become even more apparent in the analysis of the responses of the flames in Section 4.2.

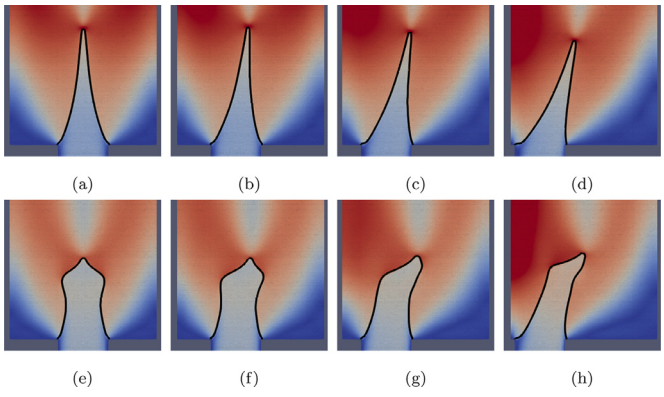

Fig. 5. Contours of the instantaneous velocity magnitude of the configurations with the excitation frequencies 50 Hz (a–d) and 100 Hz (e–h) and the excitation amplitude $a = 0.25$; The configurations are ordered from left to right: Λ_0, $\Lambda_{0.3}$, $\Lambda_{0.6}$, and $\Lambda_{0.9}$. The flame front is shown by the black contour which corresponds to $c = 0.5$.

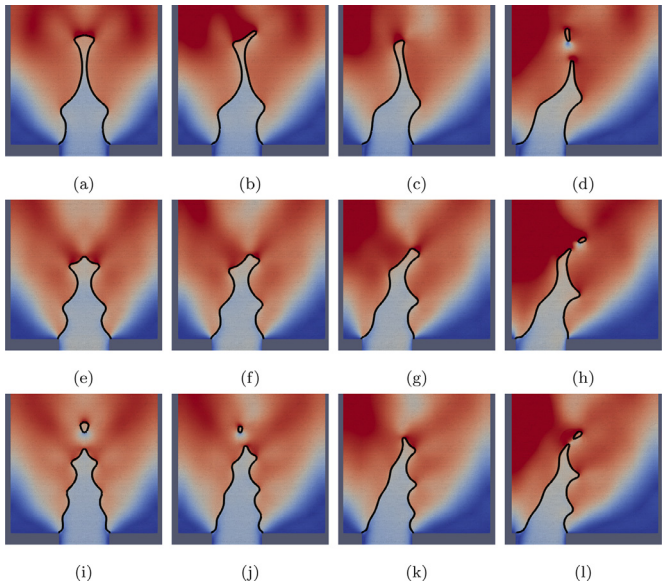

Fig. 6. Contours of the instantaneous velocity magnitude of the configurations with the excitation frequencies 200 Hz (a–d), 300 Hz (e–h), and 400 Hz (i–l) and the excitation amplitude $a = 0.25$; The configurations are ordered from left to right: Λ_0, $\Lambda_{0.3}$, $\Lambda_{0.6}$, and $\Lambda_{0.9}$. The flame front is shown by the black contour which corresponds to $c = 0.5$.

The results for the higher excitation frequencies are shown in Fig. 6. The higher excitation frequencies cause wrinkles on the flame surfaces. The wrinkles have their origin at the base of the flames and propagate along the flame surface. Since the lengths of the flanks of the flames vary in the non-symmetric configurations $\Lambda_{0.3}$ (b), $\Lambda_{0.6}$ (c), and $\Lambda_{0.9}$ (d) due to the inclination of the flames to the center of the combustion chamber, the wrinkles of each flank do not reach the flame tip at the same time. Therefore, the instantaneous wrinkle pattern on the flame surfaces varies with the position of the injector in the combustion chamber. A juxtaposition of the flame surfaces is shown in Fig. 7. Clearly, the amplitude of the wrinkles is significantly smaller on the surface of the longer flank of the flame while the amplitude is increased

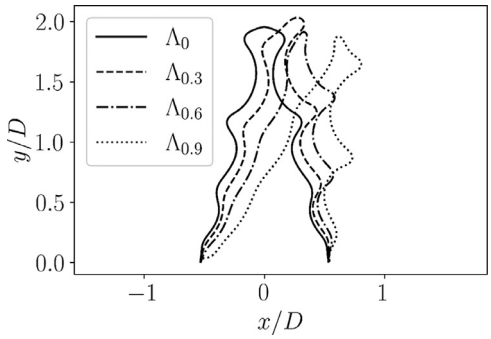

Fig. 7. Flame shapes of the steady-state solutions (a) and instantaneous solutions with the excitations frequency 400 Hz (b).

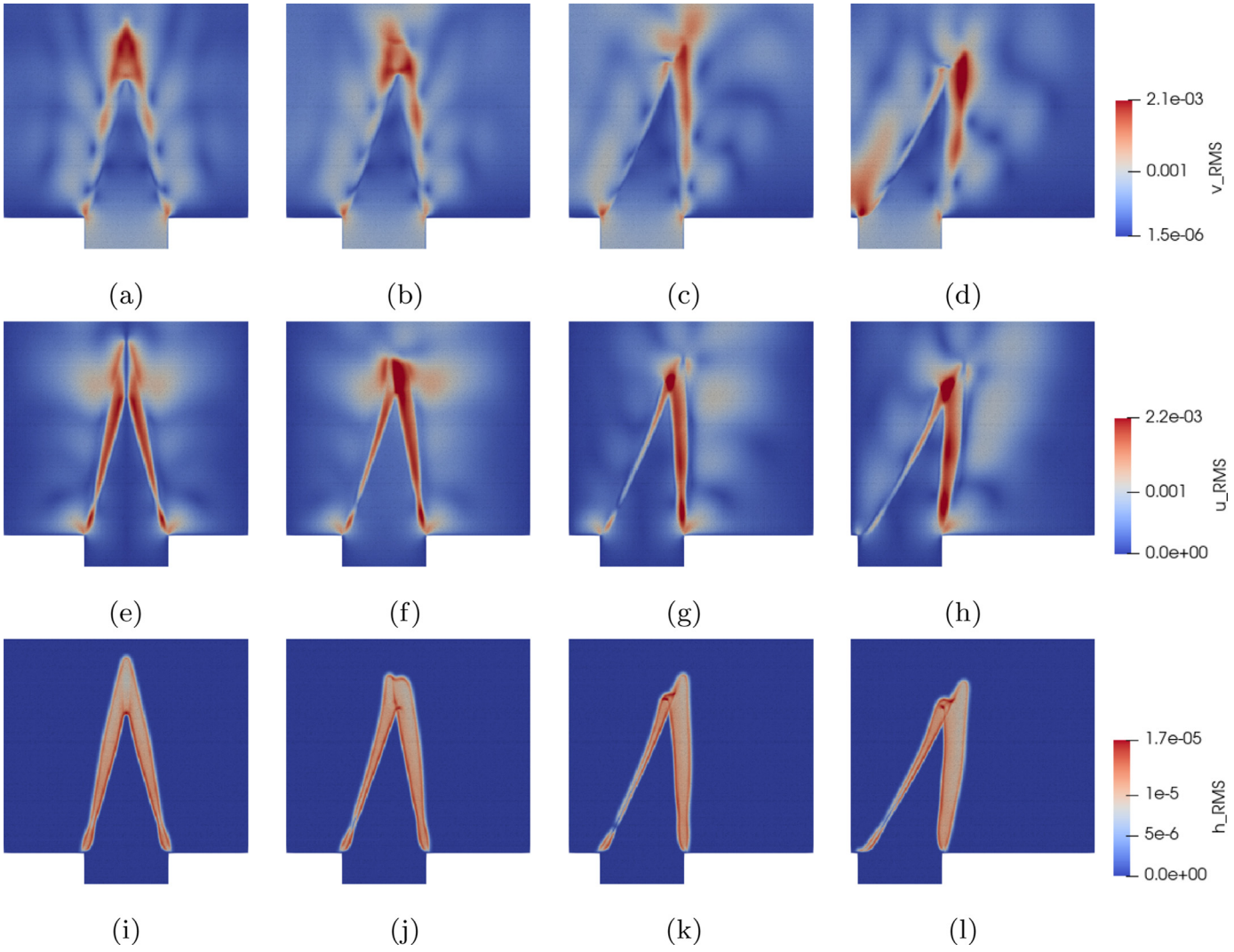

Fig. 8. Contours of the root-mean square (RMS) values of the fluctuations of the axial velocity component (a–d), the lateral velocity component (e–h), and the heat release rate (i–l).

for the shorter flank when compared to the flame of the symmetric configuration Λ_0. The high wrinkle amplitude for the shorter flanks is caused by the high excitation due to flow fluctuations, since the position of the shorter flank is close to the shear layer of the jet flow. The contours of the root-mean square (RMS) values are shown in Fig. 8 for the fluctuations of the axial velocity component (a–d), the lateral velocity component (e–h), and the heat release rate (i–l) for the excitation frequency $f = 400$ Hz. Evidently, the highest velocity fluctuations are in the tip region for the symmetrical flame. They shift towards the location of the shorter flanks of the flames for the asymmetric configurations. Consequently, the local distribution of the heat release rate changes significantly due to the lateral injector offset.

It goes without saying that the local distribution of the flame wrinkles defines the local heat release rate fluctuations which are acoustic sources of the flames. The impact of the changes of the local distribution of the flame wrinkles on the integrated heat release and the acoustic emission of the flames is discussed in the following.

4.2. Flame response to excitation

Next, the integrated heat release is shown in the figures on the left and the pressure, which defines the acoustic emission, is illustrated on the right. The integrated heat release is determined by the sum of all heat release values of the computational domain. In all the figures, the blue line corresponds to the Λ_0 configuration, the yellow line to $\Lambda_{0.3}$, the green line to $\Lambda_{0.6}$, and the red line to $\Lambda_{0.9}$. The results of the pressure are determined for each configuration at the location "MP" which is shown in Fig. 1. The exact location of "MP" has no significant impact on the results. Furthermore, note that the origin of the high frequency fluctuations in the pressure signals is not clear. However, since their frequency is much higher than the analyzed frequency range and the amplitude is relatively low the impact on the qualitative results is expected to be negligible.

The results of the lower frequency cases $f = 50$ Hz and $f = 100$ Hz with the excitation amplitude $a = 0.1$ are illustrated in Fig. 9. The findings for the lowest excitation frequency $f = 50$ Hz are depicted in Fig. 9(a) and (b). The phases and the amplitudes of the integrated heat release and the pressure signals have a low dependence on the position of the flame. For the configuration with the largest offset $\Lambda_{0.9}$ a low phase shift and a low decrease of the pressure amplitude is observed while the other pressure signals show no discrepancies. For the configurations with the excitation frequency $f = 100$ Hz in Fig. 9(c) and (d), the pressure signal of the $\Lambda_{0.9}$ configuration shows a similar discrepancy to the heat release and the pressure signals of the other three configurations.

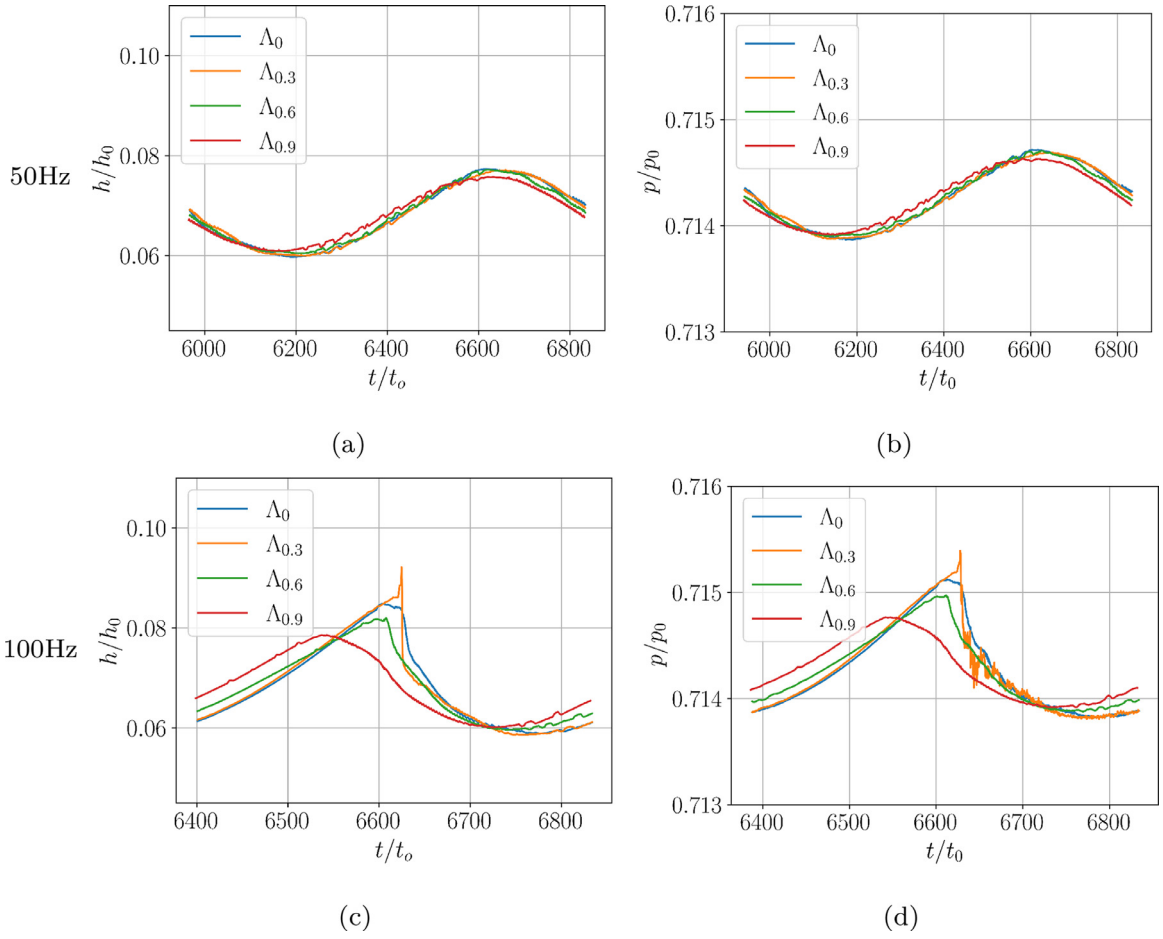

Fig. 9. The integrated heat release h/h_0 is shown on the left and the pressure signal p/p_0 at the microphone position 'MP' is shown on the right for the excitation amplitude $a = 0.1$ at low excitation frequencies; $f = 50$ Hz (a), (b) and $f = 100$ Hz (c), (d).

The phase shift to the other signals is higher than for the $f = 50$ Hz configurations. Furthermore, the amplitudes of the $\Lambda_{0.9}$ and $\Lambda_{0.6}$ configurations are lower than in Λ_0. The amplitude decreases with an increased injector position offset. Note that there is a peak in the results of the $\Lambda_{0.3}$ configuration which is caused by a small pocket. Overall, an impact for low excitation frequencies on the response of the flame is mainly evident for the largest injector position offset where the flame is positioned close to the combustion chamber wall.

The results of the higher frequency cases $f = 200$ Hz, $f = 300$ Hz, and $f = 400$ Hz are shown in Fig. 10 from top to bottom.

Evidently, the phase angle of the pressure signals and the integrated heat release are shifted for all excitation frequencies. The phase shift with respect to the symmetric Λ_0 configuration denoted as $\Delta\phi_d$, which is obtained by fast Fourier transformations of the pressure signals, is illustrated for the excitation amplitude $a = 0.1$ in Fig. 11(a). It depends on the displacement offset of the flame and on the frequency of the excitation. Note that the phase shift with respect to the Λ_0 configuration increases approximately linear by the frequency in the excitation frequency range of 200 Hz to 400 Hz. The phase shift for the excitation amplitude $a = 0.25$ is shown in Fig. 11(b). The qualitative results are the same, however, the phase angle differences depend on the excitation amplitude.

The spectra of the pressure signals obtained by fast Fourier transformations are shown in Fig. 12 for the 50 Hz configuration (a) and the 400 Hz configuration (b). As discussed above, the response of the lowest frequency configuration is linear, i.e., the spectrum of the pressure signal has a peak only at the excitation frequency. For the higher frequency configurations additional peaks are evident at multiples of the excitation frequency due to the non-linear response of the flame. Note that only the spectrum of one higher frequency configuration is shown since the qualitative results are alike for all configurations. The spectra of all configurations are available in the supplementary material. The dominant peak corresponds to the excitation frequency in all configurations, however, the relative amplitudes of the various peaks depend on the lateral offset of the injector. Therefore, in addition to the phase of the pressure signals, which was discussed before, the spectral distribution of the flame responses changes with the injector offset.

For the integrated heat release and the pressure signals with the higher excitation amplitude $a = 0.25$, the same qualitative results are evident which are depicted for the low excitation frequencies in Fig. 13 and for the high excitation frequencies in Fig. 14. The higher excitation amplitude causes a higher response of the flame at the low frequencies which results in a higher overall pressure amplitude. The amplitude of the acoustic emission of the higher frequency configurations is less impacted by the higher excitation amplitude.

In all the configurations, the graphs of the integrated heat release and the pressure signals are similar which indicates that the heat release is the main contributor to the acoustic emission of the investigated flames. The phase shift of the integrated heat release and the pressure signals is caused by the different flank lengths of the flames. The acoustic waves travel through the injector and enter the combustion chamber. Hereby, they convert into vorticity modes at the confinement jump and are transported by the mean flow field. As discussed above, due to the change of the

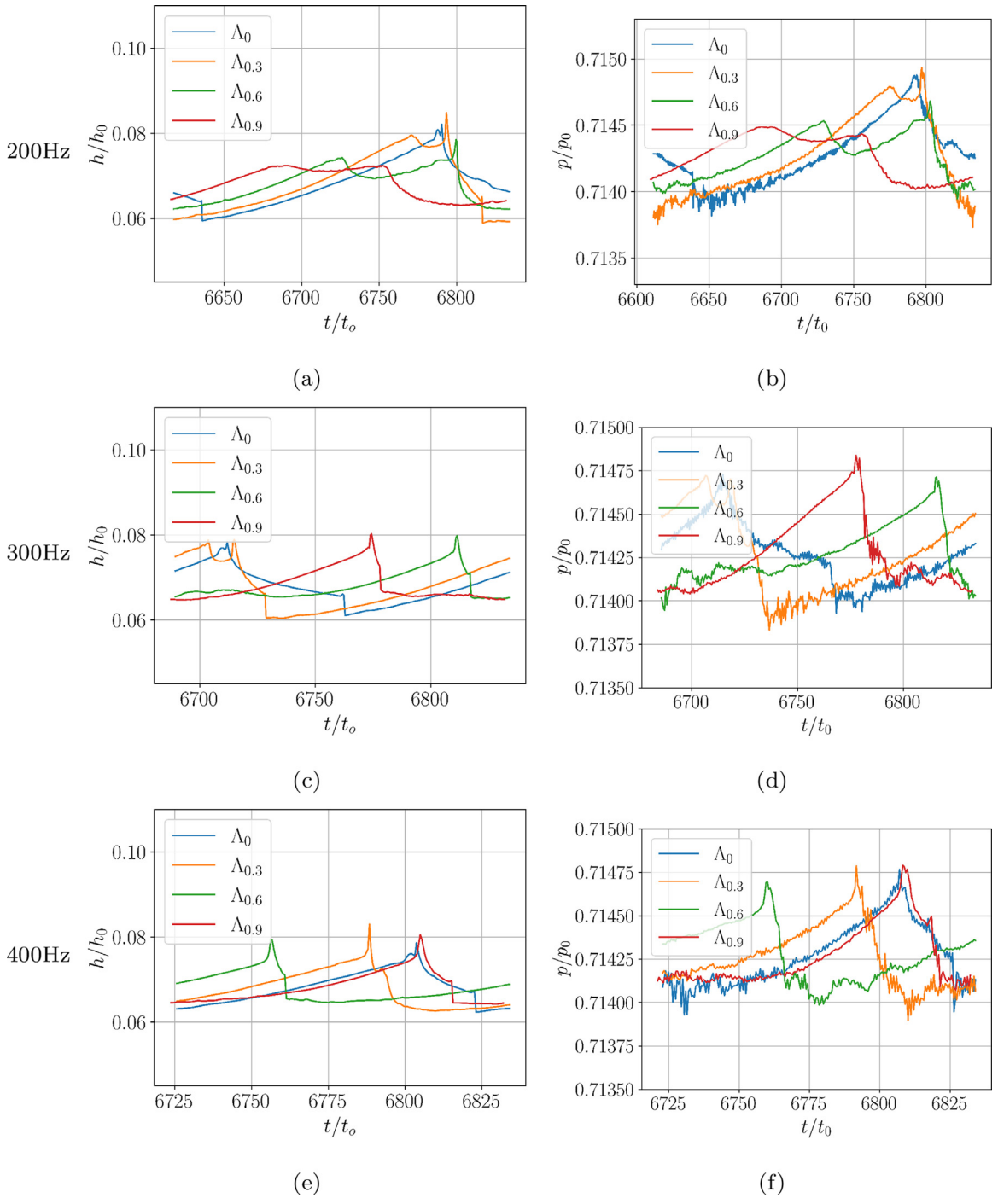

Fig. 10. The integrated heat release h/h_0 is shown on the left and the pressure signal p/p_0 at the microphone position 'MP' is shown on the right for the excitation amplitude $a = 0.1$ at high excitation frequencies; $f = 200\,\text{Hz}$ (a), (b), $f = 300\,\text{Hz}$ (c), (d), and $f = 400\,\text{Hz}$ (e), (f).

flank lengths, the resulting wrinkles on the surface of the flame have different travel distances to the flame tip on the two sides of the flame. This change of the travel distances causes a change in the local distribution of the acoustic sources which results in the shift of the response of the flames to the excitation. Since the wave number of the wrinkles on the flame surface is linear to the excitation frequency the phase shift that is caused due to the discrepancies in the travel distance of the wrinkles grows approximately linear. In the lower frequency cases in Fig. 9, this phase shift of the pressure signals is not evident since the excitation frequencies are too low to cause wrinkles on the surface of the flame. Instead, the flames move as a whole due to the high wavelength of the excitation such that the impact of the flank lengths of the flame is negligible.

Note that there are distinct peaks in the integrated heat release and the pressure signals. These peaks are caused by the formation and annihilation of flame pockets which can be seen, e.g., in the contours of the instantaneous flame fronts in Fig. 6(i). In Fig. 14(a) and (b) the integrated heat release and the pressure signals of the Λ_0 configuration and the $\Lambda_{0.3}$ configuration have one distinct peak whereas a second peak is observed in the other configurations. The second peak in the high-offset configurations is caused by the formation of a second flame pocket. Due to the different propagation times of the wrinkles at the two sides of the flame,

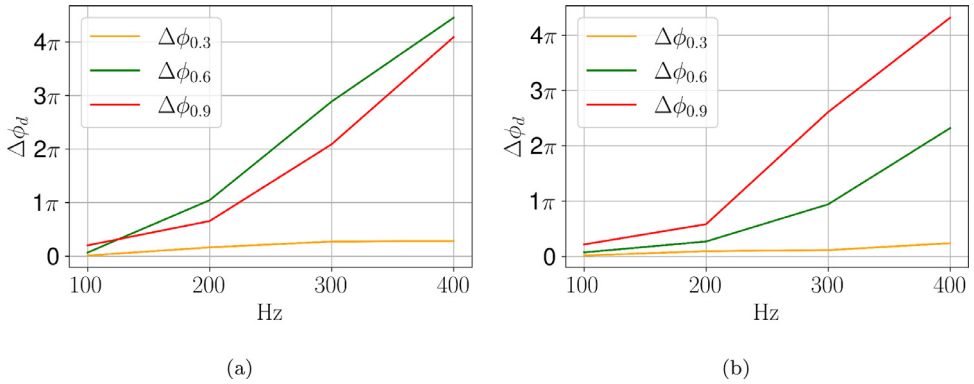

Fig. 11. Phase angle difference with respect to the symmetric Λ_0 configuration; excitation amplitude $a = 0.1$ (a) and excitation amplitude $a = 0.25$ (b).

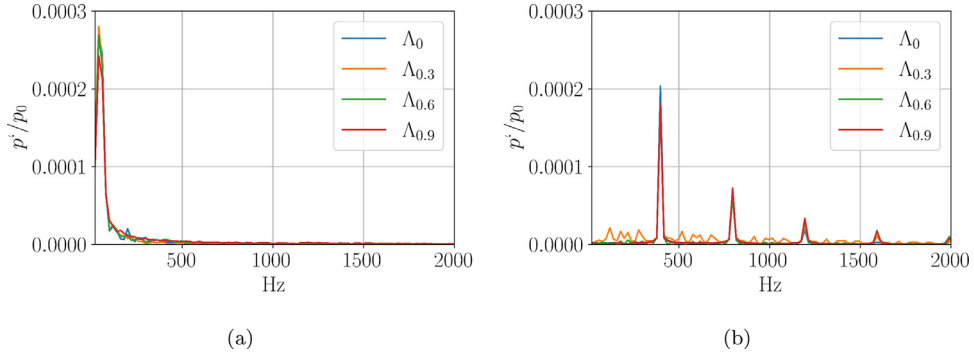

Fig. 12. Fast Fourier transformation of the pressure signals for $a = 0.1$ for the excitation frequencies 50 Hz (a) and 400 Hz (b). The results of all configurations are available in the supplementary material.

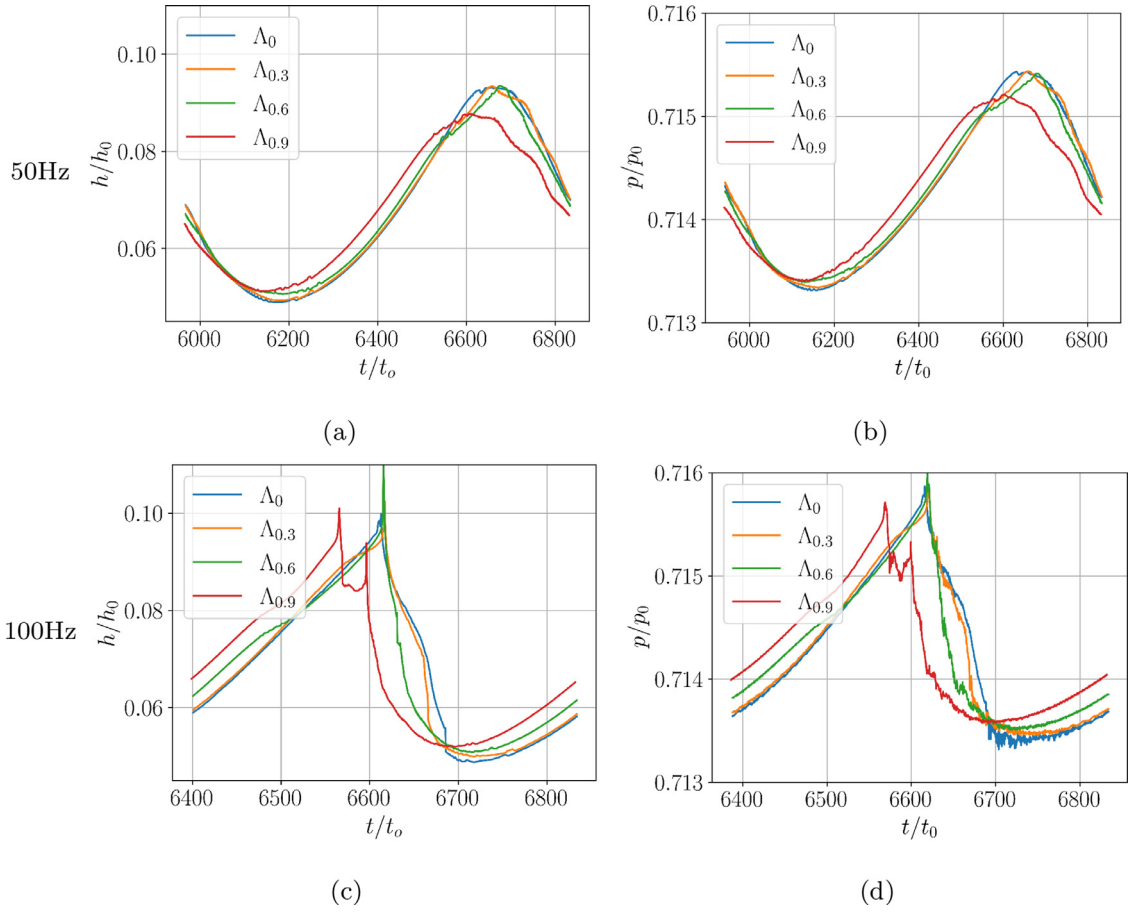

Fig. 13. The integrated heat release h/h_0 is shown on the left and the pressure signal p/p_0 at the microphone position 'MP' is shown on the right for the excitation amplitude $a = 0.25$ at low excitation frequencies; $f = 50$ Hz (a), (b) and $f = 100$ Hz (c), (d).

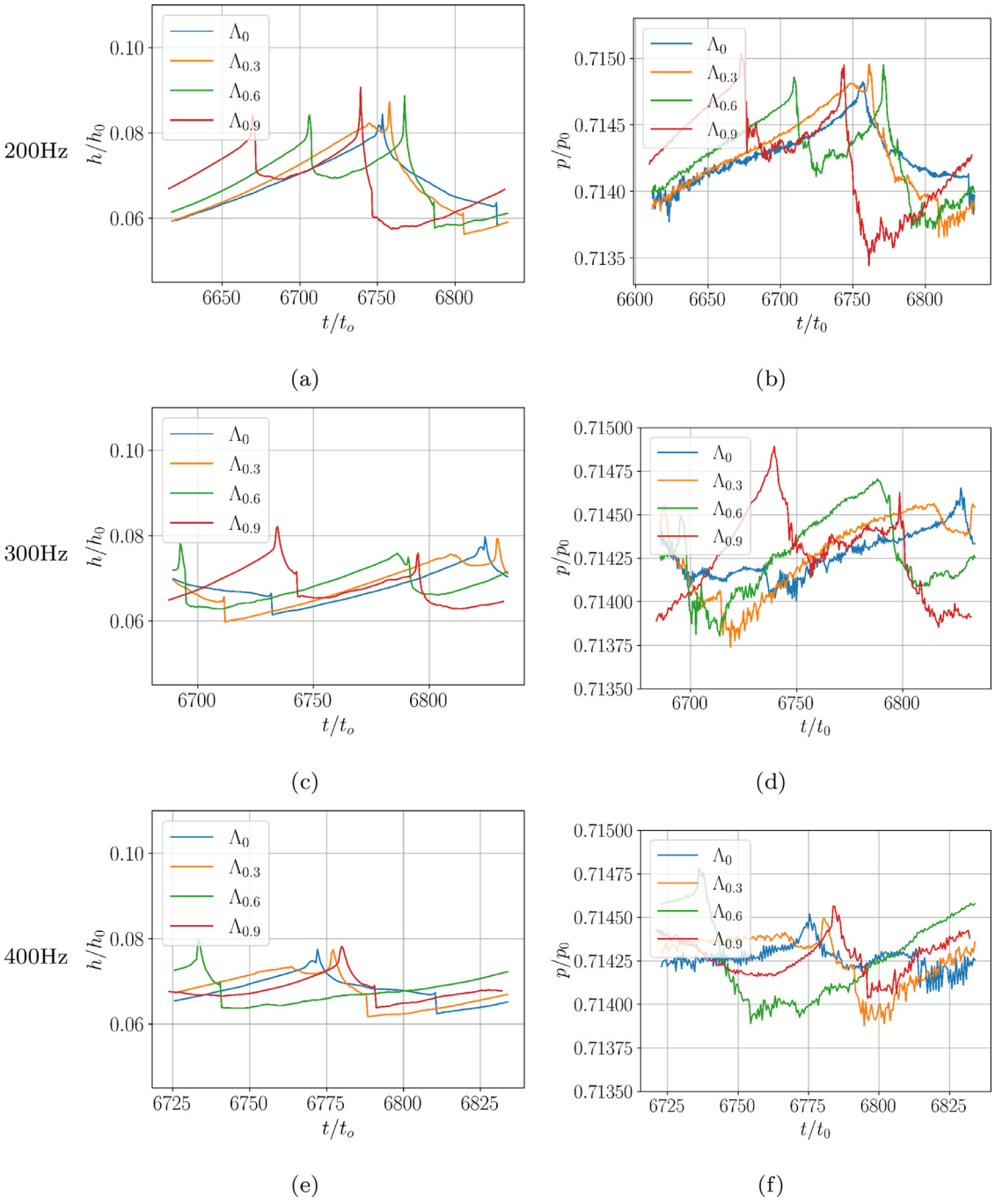

Fig. 14. The integrated heat release h/h_0 is shown on the left and the pressure signal p/p_0 at the microphone position 'MP' is shown on the right for the excitation amplitude $a = 0.25$ at high excitation frequencies; $f = 200$ Hz (a), (b), $f = 300$ Hz (c), (d), and $f = 400$ Hz (e), (f).

the tip of the flame moves from side to side and a pocket forms whenever the flame tip changes its direction of motion. The formation and annihilation of the flame pockets is best visualized in a video of the flame surfaces which is available in the supplementary material of this paper.

The significant change of the phase angle of the integrated heat release and the acoustic response of the flames due to the flame displacement offset in the combustion chamber is crucial for the stability of the burner. The phase angle of the acoustic sources of the flame determines whether or not a self-excited instability can occur at a certain frequency. Consequently, the stability of the burner can be modified by the position of the flame in the combustion chamber since the displacement offset impacts the phase angle of the flame's response to an excitation. To demonstrate that self-excited instabilities can be avoided in a real burner by changing the position of the flame in the combustion chamber, two injector positions in the combustion chamber in a configuration with more engineering boundary conditions are investigated next.

4.3. Modifying the burner stability

The stability of a burner is modified by varying the injector position offset in the combustion chamber. As explained in Section 3, the outflow boundary condition formulation is a Dirichlet boundary condition for the pressure and the length of the computational domain is increased to achieve a burner with a quarter-

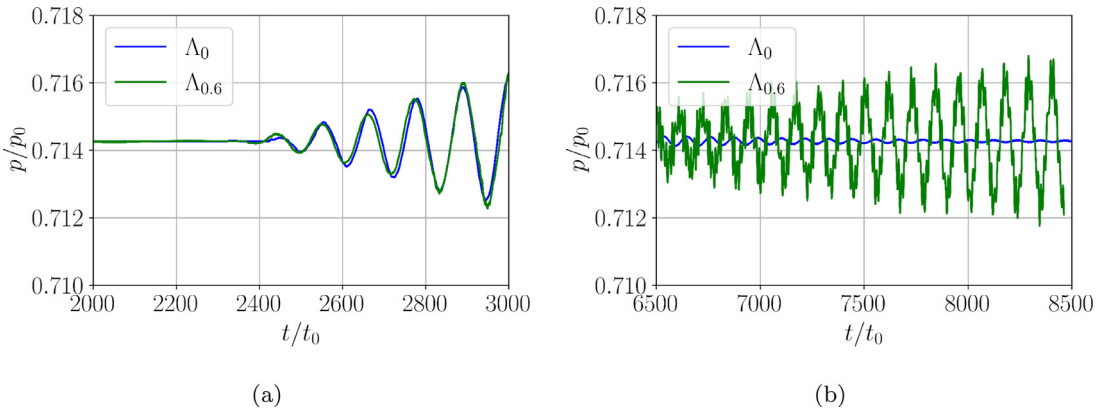

Fig. 15. Pressure signal resonance case; beginning of the excitation (a), long time after stopping excitation (b).

wave frequency of approximately 400Hz. It is evident from the results of the integrated heat release and the pressure signal in Figs. 10(e) and (f) that the flame response at $f = 400$ Hz of the Λ_0 and the $\Lambda_{0.6}$ configurations is phase shifted with respect to each other by approximately $\Delta\phi_{0.6} \approx \pi$. Consequently, a self-excited instability at 400 Hz can only occur for one of these two configurations.

To investigate the stability of the Λ_0 and the $\Lambda_{0.6}$ configurations, first, the steady state solutions of the burners are computed. Then, the quarter-wave frequency of the burner is excited by varying the inflow velocity with a frequency of 400 Hz. Finally, the excitation is stopped to analyze the coupling of the acoustic quarter-wave mode with the flame. The results are shown in Fig. 15. Evidently, the initial excitation, which is shown in Fig. 15(a), causes a high pressure amplitude in the combustion chamber of both configurations due to the resonance at the quarter-wave frequency in the combustor. However, several cycle periods after stopping the external excitation the pressure amplitudes differ significantly, which is shown in Fig. 15(b). That is, in the symmetric Λ_0 configuration the pressure amplitude decreases over time until the steady state solution is reached, whereas in the non-symmetric $\Lambda_{0.6}$ configuration the pressure amplitudes remain high due to the constructive in-phase coupling of the flame dynamics with the acoustic quarter-wave of the burner leading to a sound pressure level of approximately 143 dB.

The results show that the stability of a burner can be modified by adjusting the position of the flame in the combustion chamber.

5. Conclusions

The impact of the non-symmetric position of the flame in the combustion chamber on the response of the flame to acoustic excitations was investigated. In addition to the symmetric position, three non-symmetric flame positions were considered. The results of the steady state solutions were discussed before the integrated heat release and the pressure in the combustion chamber of the excited configurations at various excitation frequencies and two excitation amplitudes were analyzed.

Due to the change in the flow field, the flame shape of the steady flames changes with its position in the combustion chamber. That is, the tip of the flame points towards the centerline of the combustion chamber such that the lengths of the flanks of the flames depends on the injector position.

When the flames are excited wrinkles are evident on the instantaneous flame fronts for the higher frequency excitations. These wrinkles propagate along the flanks towards the flame tip. Due to the different flank lengths in the non-symmetric configurations, the wrinkles reach the flame tip at different times. Furthermore, the amplitude of the wrinkles on the longer flank tends to be lower and the amplitude on the shorter flank tends to be higher than in the symmetric configuration. Consequently, the specific injector position in the combustion chamber determines the wrinkle pattern on the surface of the flame. This wrinkle pattern constitutes an acoustic source which is underlined by the similar trends of heat release and pressure for each configuration. The amplitude of the acoustic emission of the flame is hardly affected by this. However, the phase angle is significantly altered as the flame is positioned closer to the combustion chamber wall which causes a difference of the phase angle of the integrated heat release with respect to the symmetric position of the flame. Furthermore, the phase angle difference increases approximately linearly with the excitation frequency in the frequency range of 100 Hz $< f <$ 400 Hz.

The phase angle of the response of the flame to an acoustic excitation determines the possibility of the occurrence of self-excited combustion instabilities in a burner. Based on the results of the excited flames, two injector positions were chosen in a burner configuration with a quarter-wave frequency of 400 Hz, which are mutually phase shifted by approximately π at this frequency. Therefore, it was expected that one of the configurations could exhibit a self-excited limit-cycle instability while the other configuration should be stable. The results of the simulations confirmed this assumption. Since the position of the injector impacts the phase angle of the response of the flame to acoustic excitations it can be used to modify the stability of a burner.

Declaration of Competing Interest

The authors declare that they have no known competing financial interests or personal relationships that could have appeared to influence the work reported in this paper.

Acknowledgments

The authors gratefully acknowledge the computing time granted on the supercomputer JUWELS at the Jülich Supercomputing Centre.

Supplementary material

Supplementary material associated with this article can be found, in the online version, at 10.1016/j.combustflame.2023.112995

References

[1] T. Lieuwen, V. Yang, Combustion instabilities in gas turbine engines: operational experience, fundamental mechanisms, and modeling. progress in aeronautics and astronautics series, AIAA, Vol. 210, 2005. Reston, VA

[2] A. Cuquel, D. Durox, T. Schuller, Scaling the flame transfer function of confined premixed conical flames, Proc. Combust. Inst 34 (2013) 1007–1014.

[3] A. Giauque, T. Poinsot, F. Nicoud, Validation of a flame transfer function reconstruction method for complex turbulent configurations, AIAA Paper, 2008.

[4] M. Merk, S. Jaensh, C. Silva, W. Polifke, Simultaneous identification of transfer functions and combustion noise of a turbulent flame, Proc. Combust. Inst. 37 (2018).

[5] T. Schuller, S. Ducruix, D. Durox, S. Candel, Modeling tools for the prediction of premixed flame transfer functions, Proc. Combust. Inst. 29 (2002) 107–113.

[6] T. Schuller, D. Durox, S. Candel, A unified model for the prediction of laminar flame transfer functions: comparisons between conical and v-flame dynamics, Combust. Flame 134 (2003) 21–34.

[7] P. Palies, T. Schuller, D. Durox, L.Y.M. Gicquel, S. Candel, Acoustically perturbed turbulent premixed swirling flames, Phys. Fluids 23 (2011) 037101.

[8] F. Duchaine, F. Boudy, D. Durox, T. Poinsot, Sensitivity analysis of transfer functions of laminar flames, Combust. Flame 158 (2011) 2384–2394.

[9] E. Æsøy, T. Indlekofer, G. Gant, A. Cuquel, M. Bothien, J. Dawson, The effect of hydrogen enrichment, flame-flame interaction, confinement, and asymmetry on the acoustic response of a model can combustor, Combust. Flame 242 (2022) 112176.

[10] S. Herff, K. Pausch, S. Loosen, W. Schröder, Impact of non-symmetric confinement on the flame dynamics of a lean-premixed swirl flame, Combust. Flame 235 (2022) 111701.

[11] K. Pausch, S. Herff, F. Zhang, H. Bockhorn, W. Schröder, Noise sources of lean premixed flames, Flow Turbul. Combust. 103 (2019) 773–796.

[12] H. Wang, C. Law, T. Lieuwen, Linear response of stretch-affected premixed flames to flow oscillations, Combust. Flame 156 (2009) 889–895.

[13] K. Kashinath, S. Hemchandra, M. Juniper, Nonlinear thermoacoustics of ducted premixed flames: the influence of perturbation convection speed, Combust. Flame 160 (2013) 2856–2865.

[14] A. Albayrak, W. Polifke, An analytical model based on the G-equation for the response of technically premixed flames to perturbations of equivalence ratio, Int. J. Spray Combust. Dyn. 10 (2) (2018) 103–110.

[15] C. Li, M. Zhu, J. Moeck, An analytical study of the flame dynamics of a transversely forced asymmetric two-dimensional bunsen flame, Combust. Theory Model. 21 (5) (2017) 976–995.

[16] M. Matalon, B. Matkowsky, Flames as gasdynamic discontinuities, J. Fluid Mech. 124 (2006) 239–259.

[17] D. Hartmann, M. Meinke, W. Schröder, The constrained reinitialization equation for level set methods, J. Comput. Phys. 229 (2010) 1514–1535.

[18] A. Lintermann, M. Meinke, W. Schröder, Zonal flow solver (ZFS): a highly efficient multi-physics simulation framework, Int. J. Comput. Fluid D. 0 (2020) 1–28.

[19] V. Moureau, B. Fiorina, H. Pitsch, A level set formulation for premixed combustion LES considering the turbulent flame structure, Combust. Flame 156 (2009) 801–812.

[20] S. Schlimpert, A. Feldhusen, J.H. Grimmen, B. Roidl, M. Meinke, W. Schröder, Hydrodynamic instability and shear layer effects in turbulent premixed combustion, Phys. Fluids 28 (2016) 017104.

[21] H. Pitsch, A consistent level set formulation for large-eddy simulation of premixed turbulent combustion, Combust. Flame 143 (2005) 587–598.

[22] T. Poinsot, S.K. Lele, Boundary conditions for direct simulations of compressible viscous flows, J. Comput. Phys. 101 (1992) 104–129.

[23] D.H. Rudy, J.C. Strikwerda, A nonreflecting outflow boundary condition for subsonic Navier-Stokes calculations, J. Comput. Phys. 36 (1980) 55–70.